Supporting Information

Inkjet printing of silver nanowire electrodes for fully stretchable organic light-emitting diodes

Dong Lv [a,b], Qiang Zhang [a], Xinhong Yu [a,*] and Yanchun Han [a,b,*]

[a] State Key Laboratory of Polymer Physics and Chemistry, Changchun Institute of Applied Chemistry, Chinese Academy of Sciences, Changchun, 130022, P.R. China

[b] School of Applied Chemistry and Engineering, University of Science and Technology of China, Hefei, 230026, P. R. China

Email: ychan@ciac.ac.cn (Yanchun Han)

xhyu@ciac.ac.cn (Xinhong Yu)

1. Single droplet formation of the inkjet-printed AgNW inks

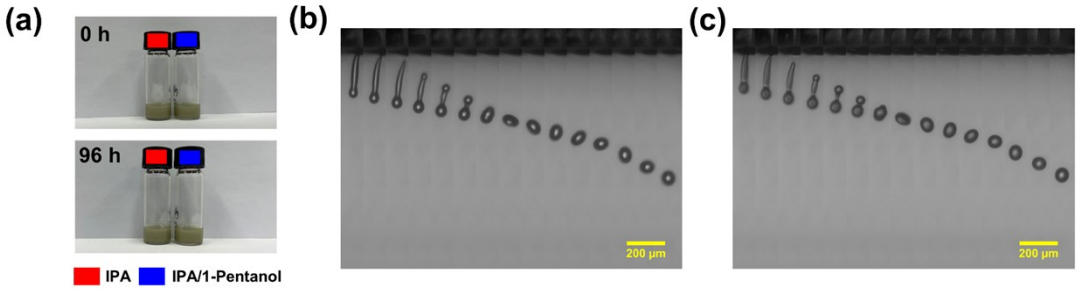

Figure S1. (a) Stability of AgNWs in IPA and IPA/1-pentanol = 80/20 (v/v) solvents. (b) Droplet formation behavior of AgNWs in IPA solvent. (c) Droplet formation behavior of AgNWs in IPA/1-pentanol = 80/20 solvent. Observation time range: 160 - 500 μs, adjacent time interval: 20 μs.

2. Surface roughness of the inkjet-printed AgNW films

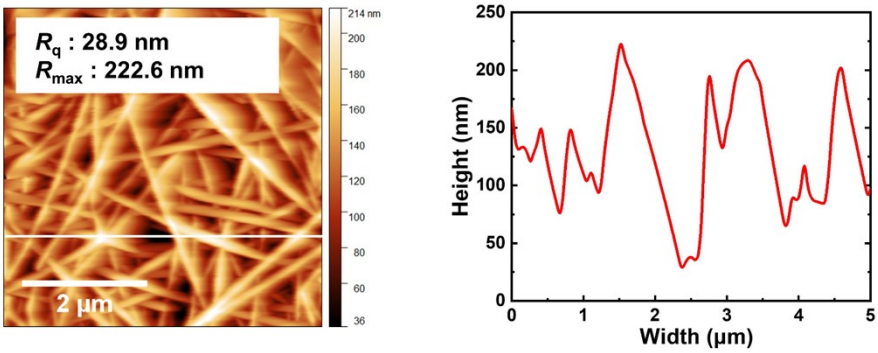

Figure S2. Atomic force microscopy height image and one-dimensional height profile of the films printed by the AgNW solutions with IPA as a single solvent.

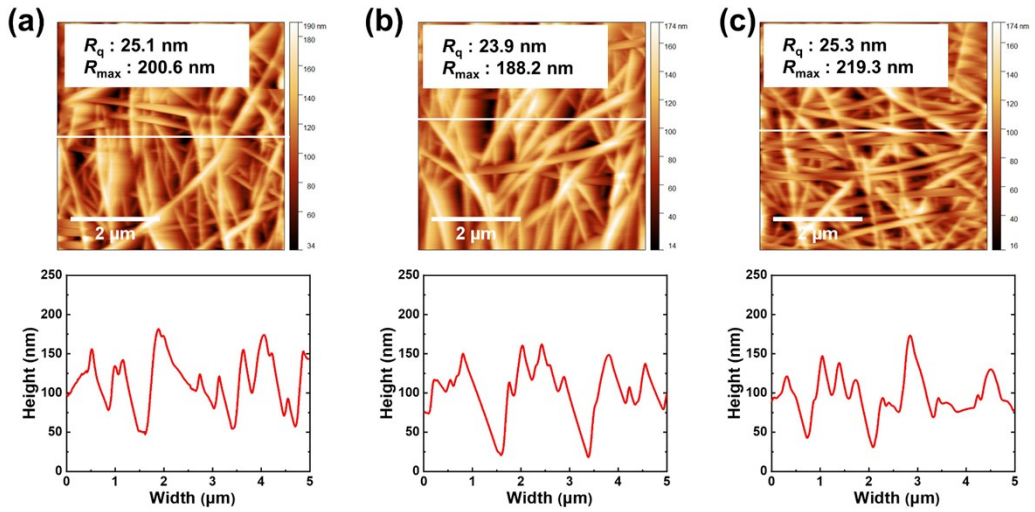

Figure S3. Atomic force microscopy height images (top) and one-dimensional height profile (bottom) of the films printed by the AgNW solutions with different ratios of cosolvents. (a) IPA/1-pentanol = 9/1. (b) IPA/1-pentanol = 8/2. (c) IPA/1-pentanol = 7/3.

3. Solvent drying time simulated by HSPIP software

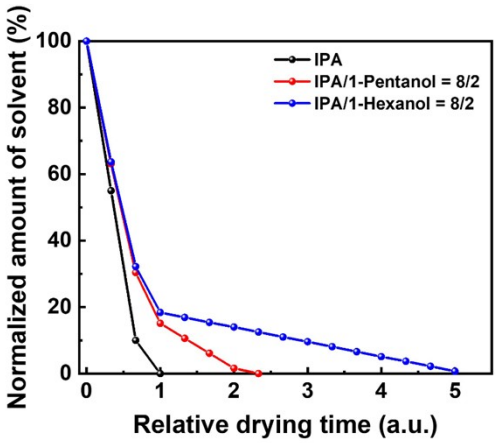

Figure S4. The relative drying time simulated with HSPiP software for pristine IPA, IPA/1-pentanol = 8/2 (v/v) mixed solvent, and IPA/1-hexanol = 8/2 (v/v) mixed solvent.

4. Roughness of the inkjet-printed AgNW electrodes after substrate transfer

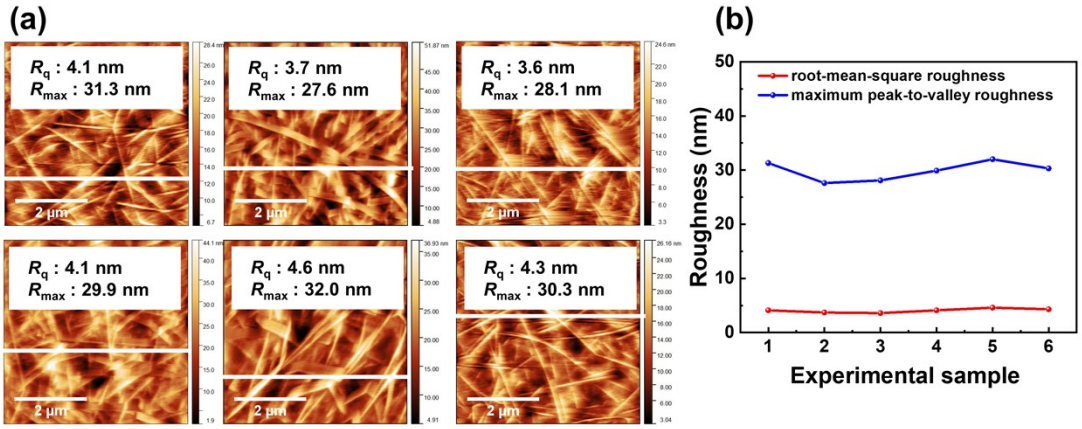

Figure S5. (a) Atomic force microscopy height image and one-dimensional height profile of the AgNW electrode surface after substrate transfer from different parallel experiments. (b) Comparison of roughness of different parallel samples.

5. Transmittance of electrodes under different strains

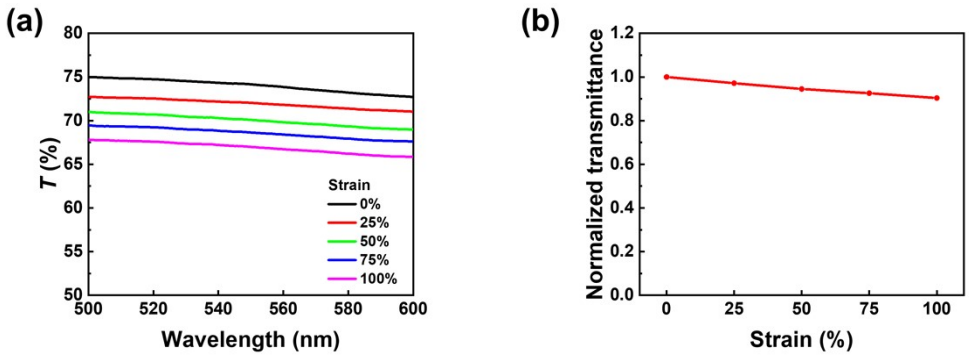

Figure S6. (a) Transmittance of the AgNW electrodes containing 0.5 mg/mL 5CB under different strains. (b) Normalized transmittance under different strains.

6. Comparison of sheet resistance of different AgNW electrodes under strain

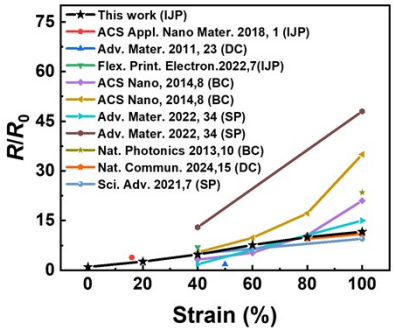

Figure S7. The R/R_0 of AgNW electrodes prepared by inkjet printing in this study under different strains compared with previous studies (where IJP is inkjet printing, DC is droplet coating, BC is rod coating, and SP is spin coating).

7. Inkjet printing of stretchable hole transport layer

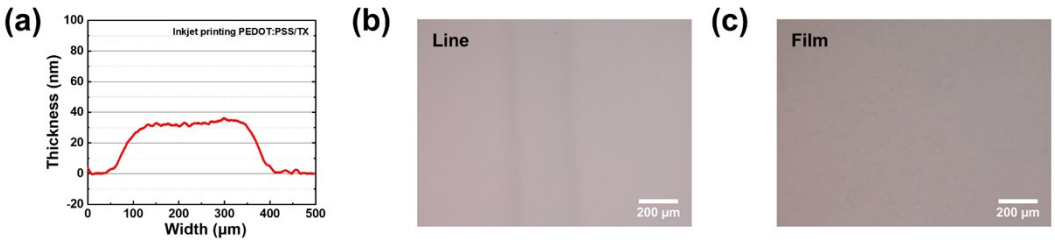

Figure S8. (a) Surface profile of the inkjet printed PEDOT:PSS/TX line pattern. (b) Optical microscopy images of line patterns. (c) Optical microscopy images of film.

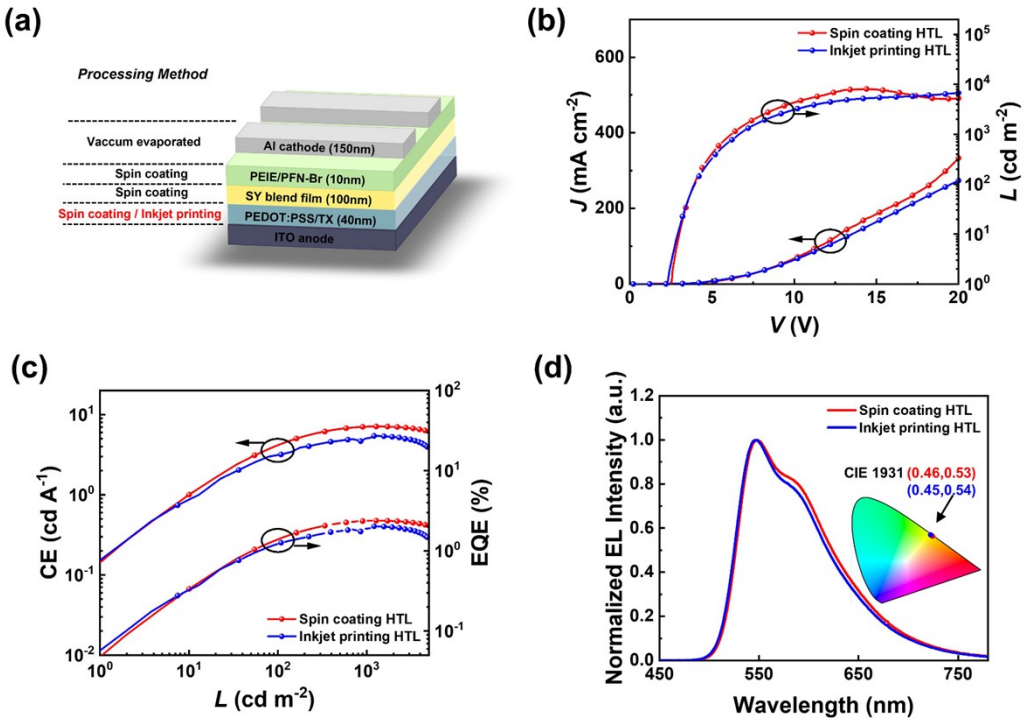

Figure S9. Comparison of device performance with PEDOT:PSS/TX films deposited by spin coating and inkjet printing. (a) Device structure. (b) Current density-voltage-luminance (*J*-*V*-*L*) curves. (d) Current efficiency (CE) and external quantum efficiency (EQE) as a function of luminance. (e) Electroluminescent (EL) spectra at the driving voltage of 7 V (inset: CIE chromaticity diagram).

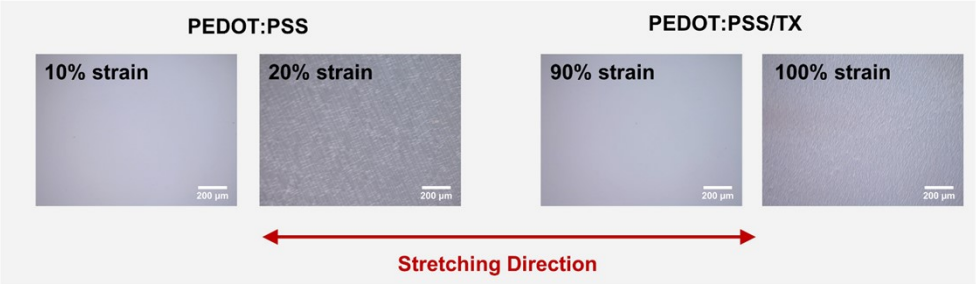

Figure S10. Optical microscopy images of PEDOT:PSS and PEDOT:PSS/TX films under different strains.

8. Inkjet printing of stretchable electron transport layer

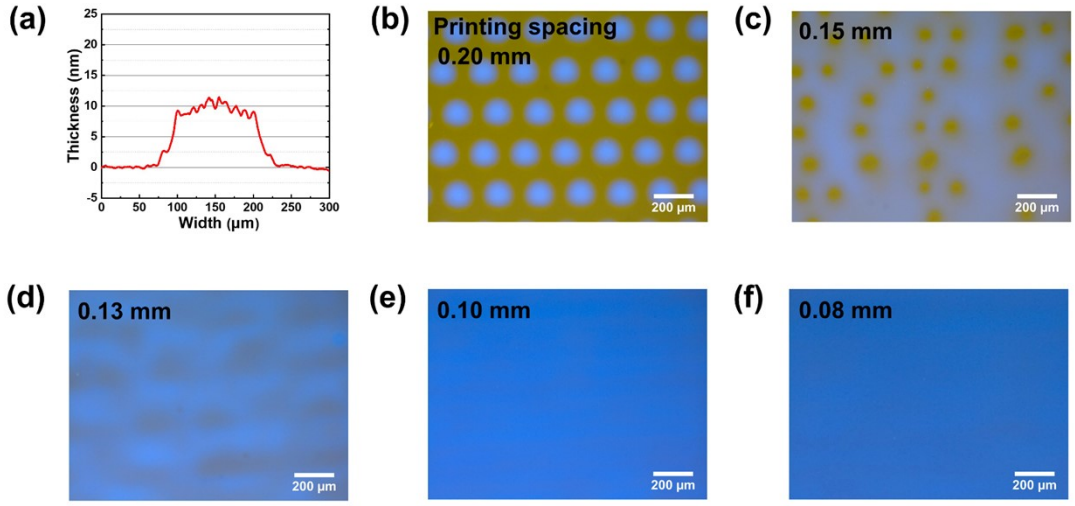

Figure S11. (a) Height profile of a single dot printed by PEIE/PFN-Br solution on EML film. Optical microscopy images of films with different printing spacing. (b) 0.20 mm. (c) 0.15 mm. (d) 0.13 mm. (e) 0.10 mm. (f) 0.08 mm.

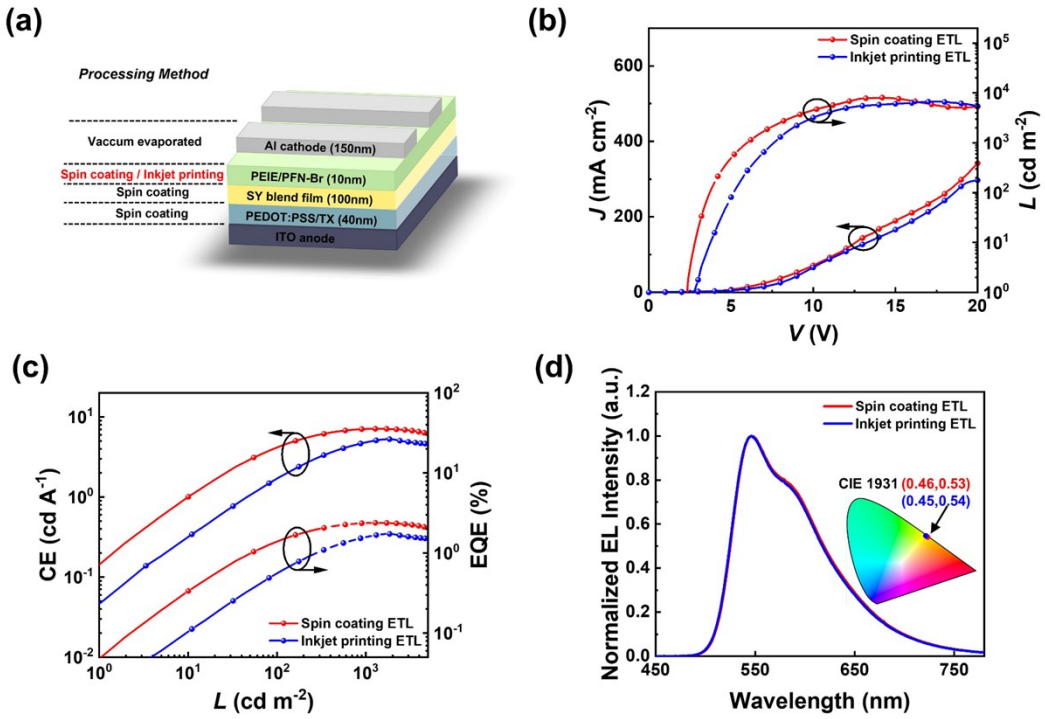

Figure S12. Comparison of device performance with PEIE/PFN-Br films deposited by spin coating and inkjet printing. (a) Device structure. (b) Current density-voltage-luminance (*J*-*V*-*L*) curves. (d) Current efficiency (CE) and external quantum efficiency (EQE) as a function of luminance. (e) Electroluminescent (EL) spectra at the driving voltage of 7 V (inset: CIE chromaticity diagram).

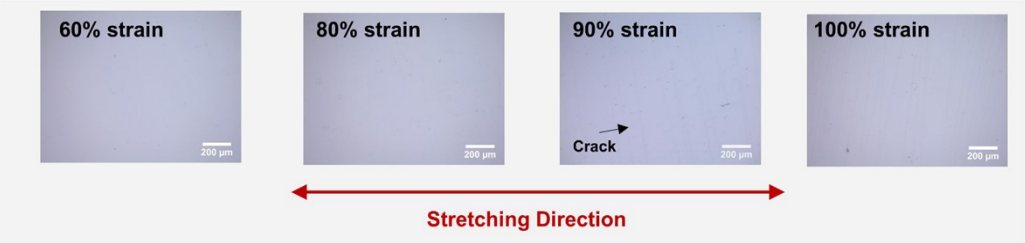

Figure S13. Optical microscopy images of PEIE/PFN-Br films under different strains.

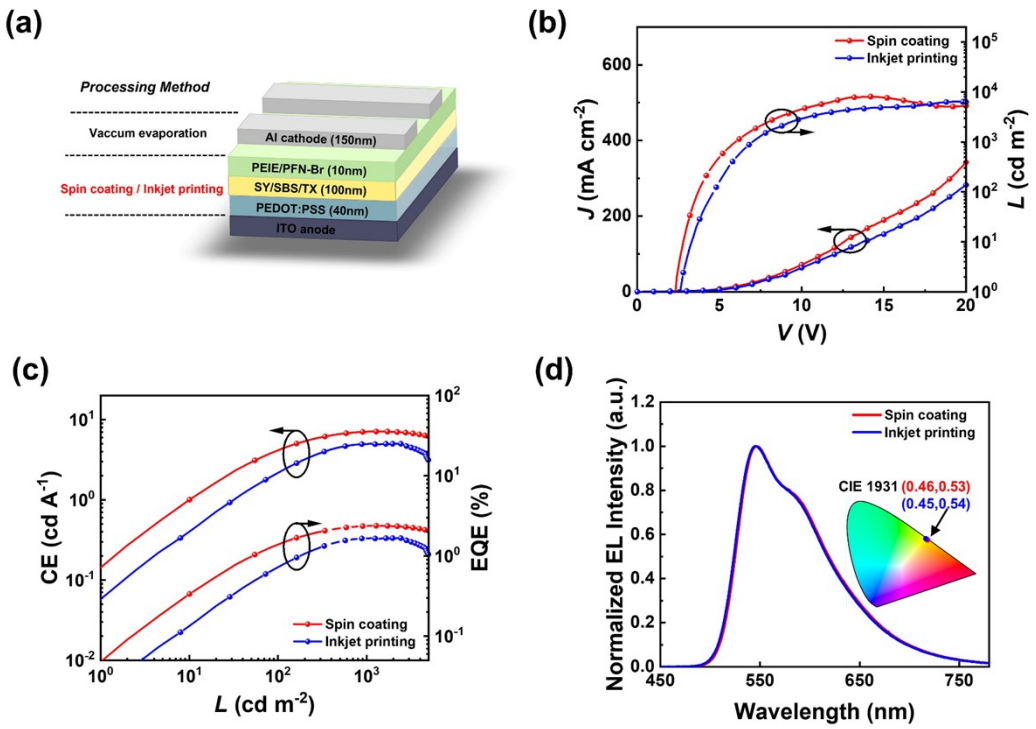

Figure S14. Comparison of device performance with multilayer films deposited by spin coating and inkjet printing. (a) Device structure. (b) Current density-voltage-luminance (*J*-*V*-*L*) curves. (d) Current efficiency (CE) and external quantum efficiency (EQE) as a function of luminance. (e) Electroluminescent (EL) spectra at the driving voltage of 7 V (inset: CIE chromaticity diagram)

9. Flowchart of the fabrication process of fully inkjet-printed stretchable OLEDs

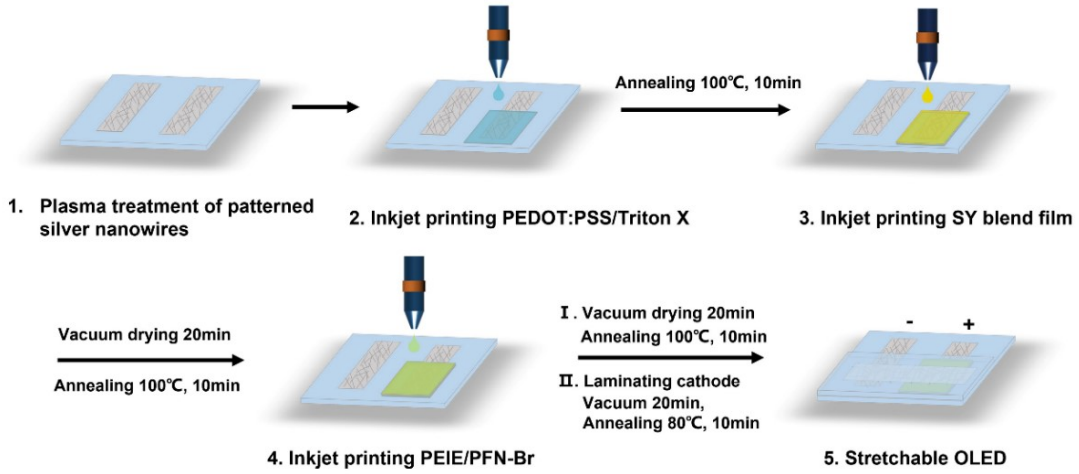

Figure S15. Flowchart of the process for fabricating the fully stretchable OLED devices using inkjet printing.

10. Optoelectronic performance of the inkjet-printed OLEDs under different strain

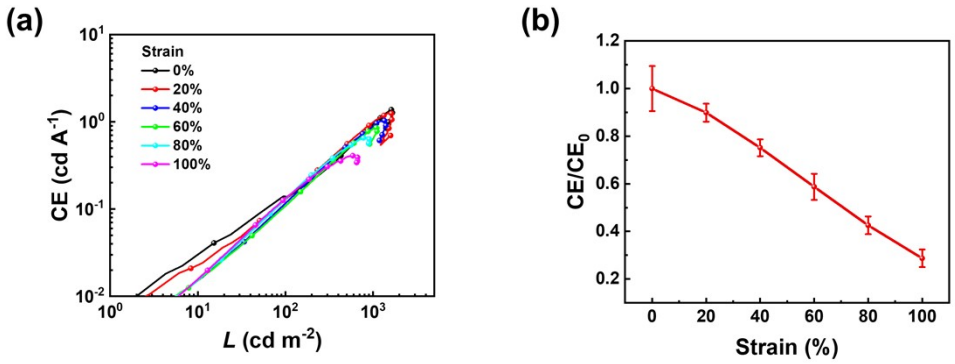

Figure S16. (a) Current efficiency-luminance (CE-*L*) characteristics of the fully stretchable OLED fabricated with the inkjet-printed 5CB-AgNW electrode under different strains. (b) Relationship between the normalized current efficiency (CE/CE_0) and strain.